Please cite the Published Version

Additional Information: This is an open access article which first appeared in Applied Materials Today

Data Access Statement: Data will be made available on request.

Advances in additive manufacturing for flexible sensors: bespoke conductive TPU for multianalyte detection in biomedical applications

Ana C.M. Oliveira [a,b], Elena Bernalte [a], Robert D. Crapnell [a], Matthew J. Whittingham [a], Rodrigo A.A. Muñoz [b], Craig E. Banks [a,*]

[a] Faculty of Science and Engineering, Manchester Metropolitan University, Dalton Building, Chester Street, M1 5GD, Great Britain, UK
[b] Institute of Chemistry, Federal University of Uberlândia, 38400-902, Uberlândia, Minas Gerais, Brazil

ARTICLE INFO

ABSTRACT

Additive manufacturing electrochemistry has the potential to revolutionise the wearable sensors industry through the rapid and customisable production of sensors; however, the currently available conductive filaments are not fit for purpose due to issues with their base polymers and filler loadings. In this work, we present the development of a highly flexible and conductive filament for additive manufacturing made with 40 wt% carbon black (CB) in thermoplastic poly(urethane) (TPU). This optimised loading of CB achieved an ideal balance between flexibility, printability, conductivity, and electrochemical performance, as demonstrated by bulk resistance measurements, TGA, SEM, XPS, Raman and through electrochemical scan rate studies, where a heterogeneous electron transfer rate constant (k^0) of 2.69 ($\pm$ 0.10) x 10^{-3} cm s^{-1} was obtained. Importantly, the electrodes exhibited great stability over 100 scans and excellent reproducibility after cleaning and re-use. Moreover, the additively manufactured electrodes were tested with the connection stem bent at five different angles, showing no deterioration of their electrochemical performance. Furthermore, we show that within the use of additive manufacturing technology, the choice of printer is key to avoid print failure; using a distance from extruder gears to nozzle, namely the filament path, as short as possible results in more reproducible additive manufacturing. Finally, the electrodes bent to the highest angle were applied to the simultaneous multianalyte detection of dopamine, uric acid and nitrite within urine demonstrating an excellent electroanalytical performance with a clear separation of the three peaks. This highly flexible and conductive material holds the potential to elevate additive manufacturing within the fields of flexible electronics and wearable electrochemical sensors.

1. Introduction

Due to rising healthcare costs globally and an ever-ageing society, there is a real drive for shifting towards preventative care and encouraging lifestyle changes rather than continuing a reactive care path. This approach aligns with the United Nations Sustainable Development Goals, within Goal 3 – "Good Health and Wellbeing", where early warning systems, as well as risk reduction, monitoring and management systems will play a crucial role. To achieve real-time, non-invasive monitoring of key healthcare variables without the discomfort and inconvenience of traditional blood analysis requires the use of wearable sensors and flexible electronics. Due to the natural variation of patients, additive manufacturing is becoming an interesting solution for producing bespoke devices tailored to individuals' needs [1,2]. It allows for the creation of unique and custom geometries on a computer-aided

design programme, which can then be translated rapidly into print files for on-demand production. To perform the analytical application of these sensing platforms, electrochemistry offers synergetic properties through its low-cost and portability, whilst also providing excellent sensitivity and selectivity.

The combination of additive manufacturing and electrochemistry, coined additive manufacturing electrochemistry, has seen a rapid rise in popularity in recent years. Among the 7 primary additive manufacturing techniques, one of the most popular to use in conjunction with electrochemical applications is Fused Filament Fabrication (FFF, also known as Fused Deposition Modelling or FDM). This technique works by extruding melted thermoplastic through a nozzle onto a print bed, building a final object in a layer-by-layer fashion. FFF has become popular within the field of electrochemistry due to its rapid prototyping capabilities, low cost, and accessibility, with excellent printers available

---

on the market for less than £500 as well as commercially available electrically conductive filaments. As a result, additively manufactured electroanalytical platforms have been increasingly reported for use within environmental analysis [3,4], patient monitoring and diagnosis [5–7], and forensic applications [8–10]. However, within the published research, the uses of commercial filament are limited to poly(lactic acid) (PLA) as the base polymer. Despite optimised designs [11,12], printing parameters [13–18], and post-print treatments [19–21], these filaments exhibit poor conductivity which translates to limited performance in electrochemical applications.

To improve the potential of additive manufacturing electrochemistry, researchers have begun to produce their own bespoke filaments with improved characteristics [22]. Due to the excellent compatibility of PLA with FFF, the majority of published work has focussed on this material. Initially, researchers simply included higher loadings of carbon within the polymer matrix [23,24], which has naturally progressed to including mixed materials to optimise the conductivity [25], material cost [26,27], or the overall functionality [28,29]. Even though these materials offer significant enhancements compared to the commercially available alternatives, they still suffer from the inherent issues of PLA; namely poor chemical stability [30] and the ingress of solution [31], which effectively makes them single-use items. To minimise the environmental impact of this, researchers have published work utilising only recycled PLA [32] and using the bio-based material castor oil as a plasticiser [33]. Even so, improving the reusability of additively manufactured electrodes remains an important step, which has led to the development of new conductive filaments based on recycled poly (ethylene terephthalate) (PETg) [34,35]. This material has shown to resist solution ingress more effectively than PLA, as well as being sterilisable via alcoholic solutions or UV treatment without compromising their electrochemical performance. Although better in this regard, PETg-based materials suffered from lower conductivity than the bespoke PLA and were also more brittle which would significantly hinder their use as wearable devices.

To produce suitable flexible electrochemical sensors through additive manufacturing, alternative materials must be investigated. Thermoplastic poly(urethane) (TPU) is a well-known material for FFF, commonly used to create highly flexible prints [36–38]. Although there is one commercially available conductive TPU filament (Ninjatek Eel), its conductivity is insufficient for electrochemical applications. TPU is a thermoplastic elastomer, which combines the properties of vulcanised rubber and the processability of thermoplastic polymers [39]. It is comprised of alternating hard and soft blocks, where the hard blocks provide multifunctional tie points, while the soft parts form an elastomer matrix accounting for the elastic properties of the material. The synergy between these interesting properties and the inherent physicochemical features of conductive carbon black particles makes this combination a promising material for a new conceptualisation of wearable sensors.

In this study, we look to produce a highly conductive TPU filament and optimise the printing conditions to develop high-performance flexible electrodes. This approach will expand the scope of additive manufacturing electrochemistry and pave the way for the production of fully additively manufactured flexible wearable sensors.

2. Materials and methods

2.1. Chemicals

All chemicals used throughout this work were used as received without any further purification. All aqueous solutions were prepared with deionised water of a measured electrical resistivity not <18.2 MΩ cm, sourced from a Milli-Q Integral 3 system from Millipore UK (Watford, UK). Hexaammineruthenium (III) chloride (98 %), potassium ferricyanide (99 %), potassium ferrocyanide (98.5–102 %), sodium hydroxide (>98 %), potassium chloride (99.0–100.5 %), sodium nitrite,

dopamine, potassium phosphate monobasic, and potassium phosphate dibasic trihydrate were purchased from Merck (Gillingham, UK). Uric acid, acetone, acetonitrile, toluene, chloroform, and dichloromethane were purchased from Fisher Scientific. Carbon black (CB) was purchased from PI-KEM (Tamworth, UK). Thermoplastic poly(urethane) (TPU, Desmopan 3855) was purchased from Hardie Polymers (Glasgow, UK).

2.2. Filament production

All TPU was dried using a hot air desiccant drier at 110 °C for a minimum of 24 h before use to remove any residual water in the polymer. The polymer compositions were prepared through the addition of appropriate amounts of TPU and CB in a chamber of 63 cm^3. The compounds were mixed using a Thermo Haake Polydrive dynameter fitted with a Thermo Haake Rheomix 600 (Thermo-Haake, Germany) at 210 °C with Banbury rotors at 70 rpm for 5 min. The resulting polymer composites were allowed to cool to room temperature before being granulated to create a finer particle size using a Rapid Granulator 1528 (Rapid, Sweden). The polymer composites were collected and processed through the hopper of a EX2 extrusion line (Filabot, VA, United States). The EX2 was set up with a single screw with two set heat zones of 60 and 210 °C, respectively. The molten polymer was extruded from a 1.75 mm die head, pulled along an Airpath cooling line (Filabot, VA, United States) and collected on a spool. After which the filament dried in a fan oven at 80 °C overnight to remove any excess moisture. The filament was then ready to use for additive manufacturing.

2.3. Physicochemical characterisation

X-ray Photoelectron Spectroscopy (XPS) data were acquired using an AXIS Supra (Kratos, UK), equipped with a monochromatic Al X-ray source (1486.6 eV) operating at 225 W and a hemispherical sector analyser. It was operated in fixed transmission mode with a pass energy of 160 eV for survey scans and 20 eV for region scans with the collimator operating in slot mode for an analysis area of approximately 700 × 300 μm, the FWHM of the Ag 3d5/2 peak using a pass energy of 20 eV was 0.613 eV. The binding energy scale was calibrated by setting the graphitic sp^2 C 1 s peak to 284.5 eV; this calibration is acknowledged to be flawed [40] but was nonetheless used in the absence of reasonable alternatives, and because only limited information was to be inferred from absolute peak positions.

Scanning Electron Microscopy (SEM) micrographs were obtained using a Crossbeam 350 Focussed Ion Beam – Scanning Electron Microscope (FIB-SEM) (Carl Zeiss Ltd., Cambridge, UK) fitted with a field emission electron gun. Secondary electron imaging was completed using a Secondary Electron Secondary Ion (SESI) detector. Samples were mounted on the aluminium SEM pin stubs (12 mm diameter, Agar Scientific, Essex, UK) using adhesive carbon tabs (12 mm diameter, Agar Scientific, Essex, UK) and coated with a 5 nm layer of Au/Pd metal using a Leica EM ACE200 coating system before imaging.

Thermogravimetric analysis (TGA) was performed using a Discovery Series SDT 650 controlled by Trios Software (TA Instruments, DA, USA). Samples were mounted in alumina pans (90 μL) and tested using a ramp profile (10 °C min^{-1}) from 0 – 800 °C under N_2 (100 mL min^{-1}).

Raman spectroscopy was performed on a DXR Raman Microscope (Thermo Scientific Inc., Waltham, MA, USA) configured with a 532 nm laser and operates using OMNIC 9 software.

Contact angles were assessed using a bespoke additive manufactured printed measurement set-up consisting of an additive manufactured stage, a Hamilton syringe, and a generic USB digital microscope connected to a computer. This equipment allowed consistent delivery of droplets to part surfaces which could be recorded as video and/or photographs using the microscope. Where possible, contact angles were analysed using ImageJ and the DropSnake plug-in [41], with reported values being the average and standard deviation of three repeat measurements.

2.4. Additive manufacturing

The filament was loaded into custom additive manufacturing equipment based on the E3D tool changer system, using E3D Hemera V6 extruder/hot-end combinations and 0.4 mm nozzles. The electrodes were printed sequentially with a rectilinear infill [14], at 238 °C and 50 °C for the nozzle and bed temperature, respectively. A borosilicate glass bed was used and covered with a thin layer of standard water-soluble glue stick to improve the adherence of TPU onto the print bed. Print speed was equalised at 10 mm/s for every print move in PrusaSlicer. This was in order to minimise any changes in inter-layer or inter-extrusion conductivity due to differences in extrusion speed. Sequential printing was chosen, as this ensures every electrode is printed identically, with no time in-between layers to cool down, as in-lab findings have shown inconsistency in electrodes printed in a traditional layer-by-layer manner. Custom GCODE was also added in-between sequential electrodes, that cleans the nozzle from any build up or contamination on in-built brass brushes in the printer.

2.5. Electrochemical experiments

All electrochemical experiments were performed on an Autolab 100N potentiostat controlled by NOVA 2.1.7 (Utrecht, The Netherlands). All electrodes printed in a standard lollipop shape were ensured to have the same diameter disc of 5 mm, connection length of 8 mm, width of 2 mm and overall thickness of 1 mm [11], and then used alongside an external commercial Ag|AgCl|KCl (3M) reference electrode with a nichrome wire counter electrode. All solutions of [Ru(NH$_3$)$_6$]$^{3+}$were purged of O$_2$ thoroughly using N$_2$ prior to any electrochemical experiments. Solutions of [Fe(CN)$_6$]$^{4-}$ were prepared in the same way without the need of further degassing.

Electrochemical impedance spectroscopy (EIS) was recorded in the frequency range 0.1 Hz to 100 kHz applying 10 mV of signal amplitude to perturb the system under quiescent conditions. NOVA 2.1.7 software was used to fit Nyquist plots obtained to adequate equivalent circuit.

Activation/glue cleaning of the additive manufactured electrodes was performed before all electrochemical experiments. This was achieved electrochemically in NaOH (0.5 M), as described in the literature for conductive PLA [42]. Briefly, the additive manufactured electrodes were connected as the working electrode in conjunction with a nichrome wire coil counter and Ag|AgCl|KCl (3 M) reference electrode and placed in a solution of 0.5 M NaOH. Chronoamperometry method was applied using a set voltage of + 1.4 V for 200 s followed by − 1.0 V for 200 s. The additive manufactured electrodes were then thoroughly rinsed with deionised water and dried under compressed air before further use.

3. Results and discussion

Within additive manufacturing electrochemistry, the majority of bespoke filament produced has utilised PLA as the base polymer due to its compatibility with additive manufacturing equipment and the presence of a commercially available conductive PLA. Although additive manufacturing lends itself well to the production of bespoke wearables, PLA does not due to its relative rigidity and ingress of solution into the polymer matrix. As such, the development of conductive filament for additive manufacturing electrochemistry requires the use of alternative polymer bases.

3.1. Production of conductive TPU filament: optimisation of carbon black (CB) loadings

TPU has been identified as a very promising polymer for the production of flexible sensors. As such, filaments with different loadings of carbon black (CB) were produced to establish the maximum possible loading and the threshold for acceptable conductivity in the electrochemical application of these composites. A schematic of filament production is shown in Fig. 1A, whereby CB and TPU are added into the chamber of a heated rheomixer, and mixed for 5 min at 210 °C. This process was followed to create blends with CB ranging from 15 wt% to 45 wt%, with the remaining weight comprised solely of TPU, as no additional plasticiser is required. Compositions higher than 45 wt% CB failed to incorporate within the polymer matrix, leaving a powder sample within the mixer. After cooling, the composites were shredded into smaller particles suitable for use in an EX2 single-screw filament extruder.

The TPU/CB composites were then extruded at 210 °C, with the different filaments collected and spooled. All the filaments that were successfully produced offered excellent low-temperature flexibility as shown in Fig. 1B and S1. Then, the diameters of each filament were consistently checked using a calliper at various points along the length of the filament. Likewise, bulk electrical resistances were also measured using a multi-meter across different 10 cm lengths of each filament (*n* = 6). This allowed comparisons to commercial and other literature benchmarks to be drawn. These results are summarised in Table 1, where it is noted that there is only one commercially available TPU with very limited conductivity. As such, a conductive commercial PLA, which is commonly found in electrochemical literature, is also shown for comparative purposes.

From Table 1 it can be seen that 5 compositions of bespoke CB/TPU are more conductive than the commercially available TPU. Additionally, the 35, 40 and 45 wt% filaments show significant improvements while outperforming the commercial PLA. This is crucial, as the electrochemical performance of commercial conductive PLA has severely limited the potential for advancing in the applications of additive manufacturing electrochemistry. The 35 wt% is a significant improvement on commercial alternatives and compares well at 104 Ω cm^{-1} to reports of conductive PLA at 86.4 Ω cm^{-1} [33] and 87.5 Ω cm^{-1} [26], and to PETg with a value of 131 Ω cm^{-1} [35]. When comparing to literature reports concerning bespoke filaments using PLA, PETg and PP, both the 40 and 45 wt% filaments compare well at 30.9 Ω cm^{-1} and 14.7 Ω cm^{-1}. The most conductive bespoke PLAs reported in the literature to date report values of 27.7 Ω cm^{-1} [27] and 24.3 Ω cm^{-1} [25], with the best PP reported at 24.7 Ω cm^{-1} and the best PETg at 71.0 Ω cm^{-1} [34]. As such, the rest of the work will focus on these three filaments.

Characterisation of the filament was then performed through thermogravimetric analysis, Fig. 1C. This provides us crucial information about the effect that the inclusion of CB within TPU has on the thermal stability of the composite, whilst also being able to confirm that the intended loadings of CB are indeed present. It can be seen in Fig. 1C that there is no significant change in the onset of degradation temperature, indicating that the presence of CB is not destabilising the polymer. When subtracting the steady state value after degradation for the virgin TPU pellet from each of the filament traces, the values of the filler percentage confirm no material loss during the manufacturing process. To understand the construction of the filament scanning electron microscopy (SEM) was performed on both the exterior of the filament, Fig. 1D, and the internal cross section of the filament, Fig. 1E. The external surface of the filament in Fig. 1D shows a smooth surface attributed to the TPU polymer, with the presence of some undulations, which is thought to be due to the presence of CB. There is a stark difference when comparing to the internal cross section, Fig. 1E. In this micrograph there is a clear presence of aligned and stretched polymer with large quantities of intercalated spherical CB particles. This indicates that there is a large amount of polymer that migrates to the surface of the filament upon extrusion, encasing the carbon black.

3.2. Print optimisation for conductive TPU filament

Due to the nature of highly flexible materials, such as TPU, the choice of printer and especially the choice of extruder is particularly important. It is preferable to use an extruder/hot-end setup with the smallest distance between the extruder gears and nozzle as possible. It is also
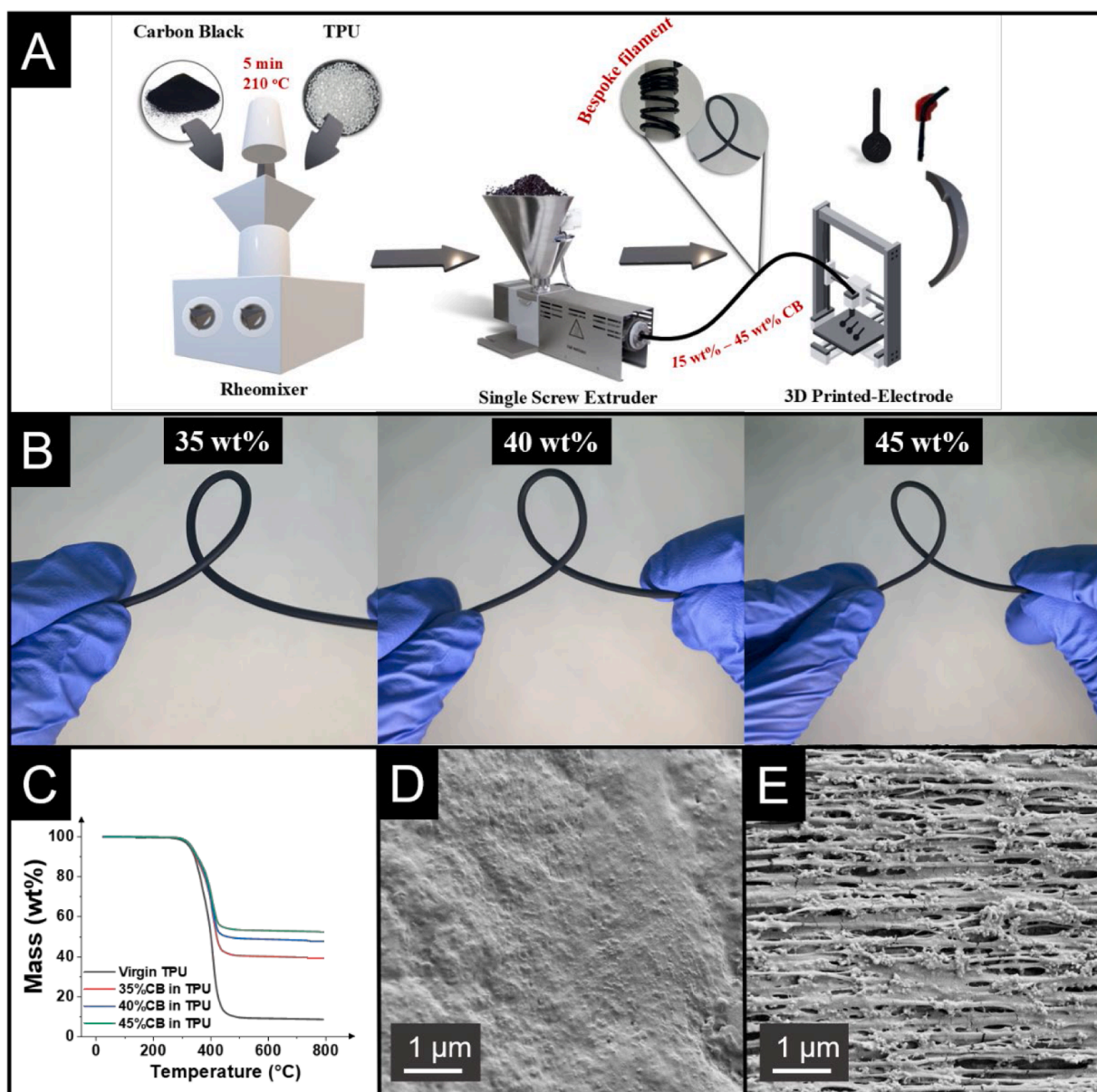
Fig. 1. A) Filament production scheme. **B)** Photographs highlighting the low temperature flexibility of the 35, 40 and 45 wt% CB/TPU filaments. **C)** Comparison of the thermogravimetric analysis (TGA) of the virgin TPU and the 35, 40 and 45 wt% CB filaments produced. SEM micrographs of the **D)** surface and **E)** cross-section of the 40 wt% CB/TPU filaments.

Table 1
Comparison of the diameters and resistances for the bespoke CB/TPU filaments against commercial alternatives.

Filament	Diameter (mm)	Resistance (Ω cm^{-1})
15 wt% CB	1.65 ± 0.05	–
20 wt% CB	1.80 ± 0.08	2575 ± 306
25 wt% CB	1.70 ± 0.08	644 ± 84
30 wt% CB	1.70 ± 0.09	539 ± 68
35 wt% CB	1.65 ± 0.05	104 ± 8
40 wt% CB	1.65 ± 0.04	31 ± 4
45 wt% CB	1.65 ± 0.06	14.7 ± 0.3
Commercial TPU	1.75	754 ± 49
Commercial PLA	1.75	380 ± 15

critically important to ensure the filament path from extruders to the nozzle is as well constrained as possible. In general, less current 3D printers tend to use a single gear bowden extruder (Figure S2A), or a dual gear bowden extruder (Figure S2B), whereas more current 3D printers (such as the Prusa i3 MK3S+) typically use dual gear direct-drive extruders (Figure S2D) and seldom employ single gear direct-drive extruders (Figure S2C). Dual gear direct-drive extruders are the most recommended for flexible materials due to the shorter filament path, and greater forces they can apply to the filament by driving it from two sides.

Concerning the anatomy of the extruder and hot-end within a 3D printer, the extrusion process of very low shore hardness materials (highly flexible and "soft") is analogous to pushing a piece of elastic through a tube. In this scenario, if the tube is much larger than the elastic, the elastic will bend, twist and bunch up on itself, making it difficult to push through the tube. However, should the tube be fractionally larger than the elastic, it is significantly easier to push the elastic through the tube, as it has no room to bend or bunch on itself. Specifically, observing the 3D printed construction of the Prusa i3 MK3S+ extruder's path (Fig. 2A), which was another 3D printer tested in this work, the filament is guided from the extruder gears to the heat-break
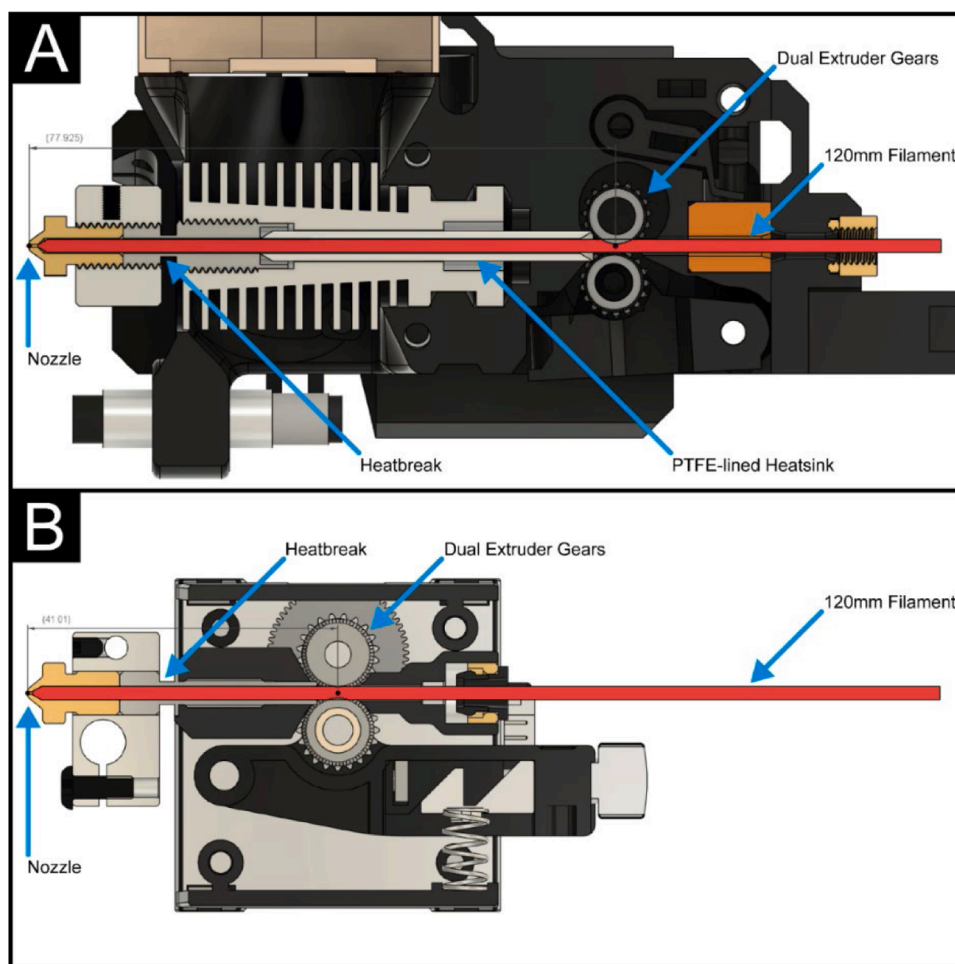
Fig. 2. A) Cross-section representation of length of 120 mm filament (1.75 mm diameter) inside the Extruder & Hot-end of the Prusa i3 Mk3s+. **B)** Cross-section representation of length 120 mm of filament (1.75 mm diameter) inside the E3D Hemera (Hermes) V6 Extruder and Hotend.

via a PTFE tube (so called PTFE-lined heatsink) that has an interior diameter of 2 mm [43]. Given the nominal filament diameter of 1.75 mm, this allows 0.25 mm of movement between the sides of the filament and the interior of the tube. However, filament and PTFE tubes are both subject to manufacturing tolerances. Theoretically, given the standard stated tolerances of ± 0.05 mm, this movement gap could be as high as 0.35 mm. From the PTFE tube, the filament is passed through the heat-break, directly into the nozzle. In this case, the distance from extruder gears to nozzle (namely the filament path) is approximately 78 mm.

In contrast, the E3D Hemera V6 extruder and hot-end setup (Fig. 2B) has precision machined aluminium and injection moulded parts, therefore the filament travels straight from the extruder into the heat-break (internal diameter ~1.8 mm), as the heatsink (PTFE lined component in the Prusa i3 MK3S+) is now integrated into the extruder body [44]. This gives a total filament path, from extrusion gear to nozzle, of only 41 mm. As the volumetric amount of molten filament extruded is a crucial factor in the success and accuracy of a 3D printed part, this extra space can cause more or less filament to be extruded than is requested by the GCODE print file, leading to failed or poor prints. Additionally, slack in the bowden tube of a bowden extruder can seriously affect the performance of the print's retraction movements, leading to stringy, poorly defined prints when using flexible filaments.

Taking all of this into account, it is unsurprising that it was difficult to produce consistent prints using a Prusa i3 MK3S+ and therefore the filament was loaded into a custom 3D-printer based on the E3D tool changer system, using E3D Hemera V6 extruder/hot-end combinations

and 0.4 mm nozzles. The electrodes were printed sequentially, at 238 °C and 50 °C for the nozzle and bed temperature, respectively. A thin layer of glue was applied to the print beds to further aid with print adhesion. It was found that the 35 wt% and 40 wt% CB/TPU filaments printed excellently, however it was not possible to produce a reproducible print using the 45 wt% filament due to a poor extrusion and difficult bed adhesion. As such, only the 35 wt% and 40 wt% additive manufactured electrodes were investigated further.

3.3. Physicochemical characterisation of printed TPU electrodes

Once printed, it was important to physicochemically characterise the printed electrodes. Initially, to establish whether the use of glue on the print bed during the printing process affected the surface of the electrodes, contact angle measurements were performed. Fig. 3A and B show the contact angle measurements for an electrode printed from the 40 wt % CB/TPU on the bottom side that was adhered to the print bed (with glue) and the top of the print (without glue), respectively. It can be seen that there is a significant difference between the two images with an angle of 110° measured for the top side without glue and an angle of 84° measured for the bottom side with the presence of glue. This clearly indicates the influence of the layer of water-soluble glue on the bottom side of the electrode as well as a very different surface structure naturally produced after printing, which will both have a significant impact on the electrode|solution interface and therefore the overall electrochemical performance of the electrode. To remove the glue and normalise the surface on both sides of the electrode, a cleaning process
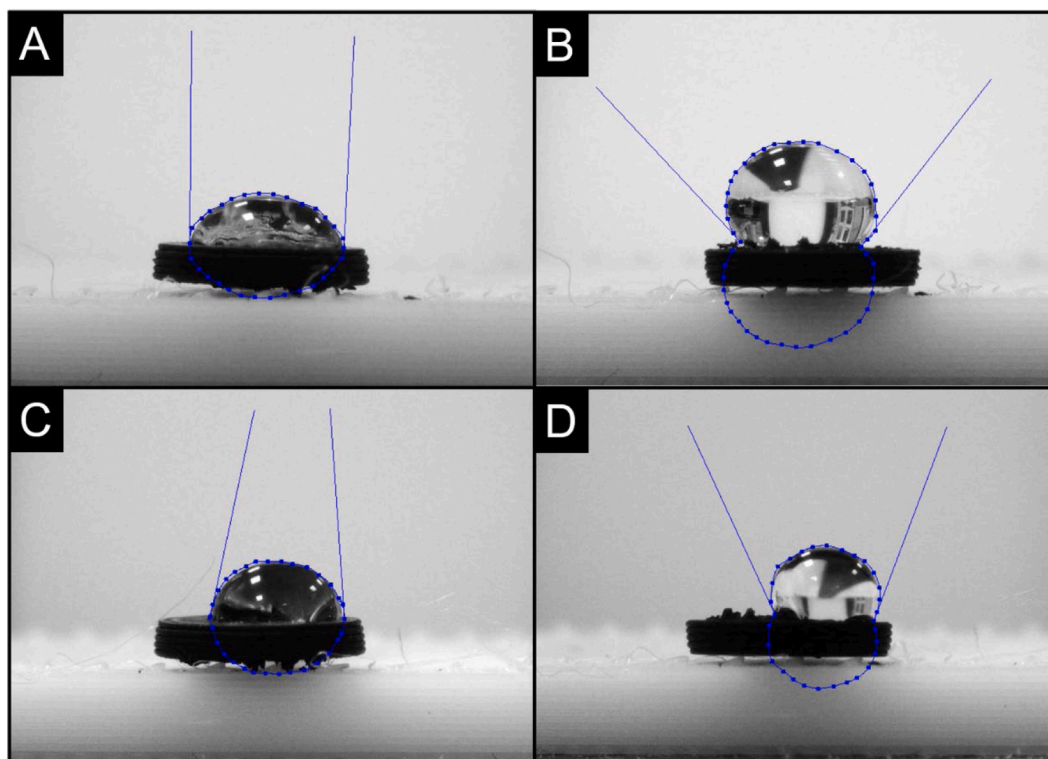
Fig. 3. Contact angle measurements performed for the conductive 3D printed electrode (40 wt% CB/TPU filament based) using water as a solution (*n* = 3) before cleaning **A)** bottom electrode, **B)** top electrode; after cleaning **C)** bottom electrode, **D)** top electrode.

was carried out. Internal unpublished results have shown that this method effectively removes glue from conductive polypropylene electrodes. By using the same procedure, which involves applying chronoamperometry within 0.5 M NaOH, as commonly used to activate conductive PLA electrodes [42], the glue was successfully removed, leading to an improvement in the contact angles for both sides of the electrodes, as shown in Fig. 3C and D.

It is important to establish what effect the printing and cleaning procedures have on the surface of the additive-manufactured electrodes. As such, X-ray photoelectron spectroscopy (XPS) was performed on both as-printed and cleaned electrode obtained using 40 wt% CB/TPU filament, as well as on virgin TPU pellet to understand how the CB is affecting the surface. Fig. 4A and B show the C 1 s spectrum for the as-printed and cleaned electrodes respectively, with the survey scans, O 1 s spectra and TPU pellet data found within Figure S3. Within the survey scans found in Figure S3A, S3D, and S3F, it is observed that in all three samples there is the presence of carbon, nitrogen, and oxygen, which are all expected from the known structures of TPU and CB. Within the cleaned 40 wt% sample the presence of a small amount of Na can be found, which is attributed to the NaOH solution used for cleaning (Figure S3F). When fitting the C 1 s spectra for the virgin TPU pellet (Figure S3B), 5 symmetric peaks were required for an appropriate fit, with one major peak corresponding to the C—C sp^3 bonding at 285 eV, and then three minor peaks attributed to the C—O, C=O, and O—C=O bonding expected from the structure of TPU. There was a requirement for an additional adventitious carbon peak (Adv C) to be fitted, which is a thin layer of carbonaceous material that is commonly found on the surface of most air exposed samples [45,46]. When comparing the C 1 s fit for the 40 wt% CB/TPU as-printed electrode (Fig. 4A), an additional asymmetric peak was required at 284.5 eV, which is assigned to the X-ray photoelectron emission of graphitic carbon [47,48]. After the cleaning process, there is an expected significant increase in the magnitude of this asymmetric graphitic peak, Fig. 4B, corresponding to an increase in atomic concentration to 36.5 % from 5.1 % in the

as-printed sample. This indicates that the cleaning procedure is not only dissolving the glue layer but also removing surface polymer from the printed electrode, exposing larger amounts of the sp^2 hybridised carbon embedded beneath.

To further examine the material, Raman spectroscopy was performed on both the as-printed and cleaned samples, as depicted in Fig. 4C and D. Within both samples, there are clearly defined peaks present at 1338 and 1572 cm^{-1}, which are attributed to the characteristic D- and G- bands found within the Raman spectra for graphitic-like structures. Through calculating the I_D/I_G ratio within the spectra of 1.01, the presence of CB on the surface can be confirmed. The presence of smaller, less well-defined peaks at 2680 cm^{-1} and 2928 cm^{-1} can be attributed to the 2D-band for the graphitic structures from carbon black and C—H stretching vibrations within the CH$_2$ groups on the polymer, respectively [49] which grows relatively in magnitude (compare Fig. 4C and D) when activated. To confirm these findings SEM was performed on the surface of both electrodes, Fig. 4E and F. Similarly to the surface of the filament seen in Fig. 1D, the as-printed electrode shows a smooth coverage of polymer material with some undulations due to the presence of small amounts of underlying CB. For the cleaned electrode, Fig. 4F, these characteristics are still present although there are some more notorious surface perforations in the polymer film, which suggests that more CB will be present and accessible on the surface.

3.4. Electrochemical characterisation of TPU electrodes

Once physicochemically characterised, the electrodes were electrochemically tested. Firstly, the electrodes were tested against the near-ideal outer-sphere redox probe hexaamineruthenium (III) chloride ([Ru(NH$_3$)$_6$]$^{3+}$) before and after the cleaning process, Fig. 5A. It is clear that the cleaning process significantly helps to create a surface for an improved electrochemical performance. As such, only electrodes cleaned using the methodology previously described were studied further. A comparison with commercial TPU is also depicted in Fig. 5A
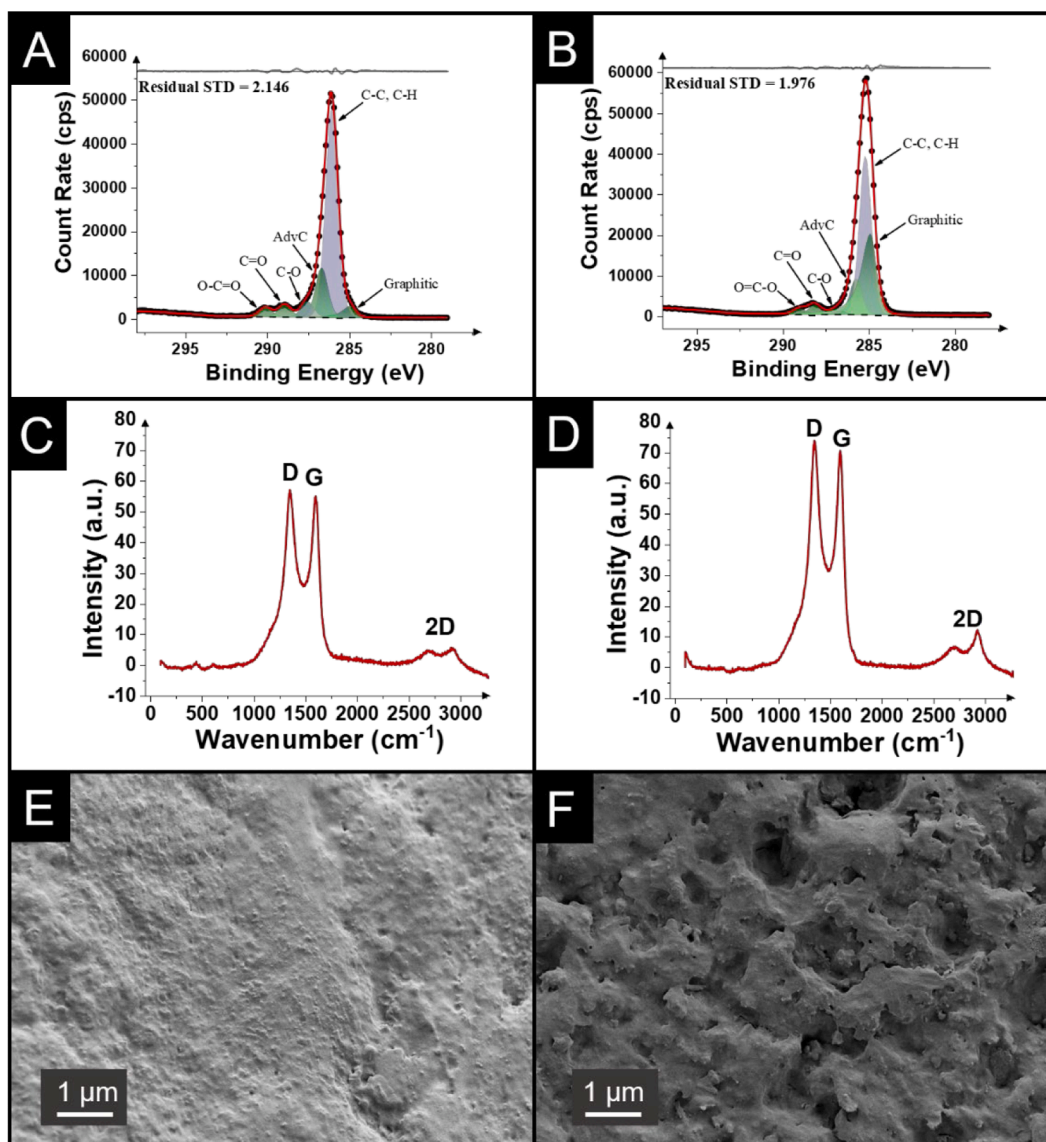
Fig. 4. XPS C1 s data of the 40 wt% CB/TPU electrodes **A)** before and **B)** after cleaning. Raman spectra for the **C)** as-printed and **D)** cleaned 40 wt% CB/TPU electrode. SEM images of the 40 wt% CB/TPU electrodes **E)** before and **F)** after cleaning.

showing that our bespoke 40 wt% CB/TPU outperforms the only available commercial conductive TPU, which effectively gives no electrochemical response. Next, the electrodes were electrochemically benchmarked using scan rate studies against $[Ru(NH_3)_6]^{3+}$ as this allows for the best determination of the heterogeneous electron (charge) transfer rate constant (k^0) [50,51].

Fig. 5B shows an example of the cyclic voltammograms ($\nu = 5 - 500$ mV s^{-1}) obtained using the 40 wt% CB/TPU filament, with the 35 wt% shown in Figure S4. Inset is the associated Randles-Ševčík plot confirming the diffusion-controlled nature of the redox process. From these experiments it was possible to find the peak-to-peak separation (ΔE_p) and k^0, which are summarised within Table 2. For the 40 wt% electrode, a k^0 value of 2.69 ± 0.10 cm s^{-1} was obtained, which compares favourably to the literature reports for bespoke conductive PP at 2.00 ± 0.04 cm s^{-1} [52] and conductive PLA at 1.7 ± 0.2 cm s^{-1} [25] for electrodes of identical geometries. Importantly, the electrodes printed from both 35 and 40 wt% CB/TPU gave highly reproducible voltammograms, which can be observed according to the standard deviations indicated in the associated Randles-Ševčík plot.

To further evaluate the electrochemical performance, scan rate studies (15–150 mV s^{-1}) were performed against the commonly used

inner-sphere redox probe $[Fe(CN)_6]^{4-}$ (1 mM in 0.1 M KCl). Fig. 5C shows an example of the cyclic voltammograms obtained. From this and the results in Table 2 it is clear that 40 wt% CB/TPU gives an improved performance both for the outer and inner sphere redox probes. Next, the electrodes were analysed using electrochemical impedance spectroscopy (EIS) in $[Fe(CN)_6]^{4-/3-}$ (1 mM in 0.1 M KCl). This powerful technique allows us to elucidate both the solution resistance (R_S) and the charge-transfer resistance (R_{CT}) of the additive manufactured electrodes. Fig. 5D shows a comparison of the Nyquist plots obtained for both electrodes, where it can be seen that the 40 wt% electrode gives an improved performance both in terms of a lower R_S and R_{CT}.

One issue that arises with additive manufactured electrodes printed using PLA is stability over time due to its poor chemical resistance [30] and the ingress of solution into the polymer matrix [31]. As such, the stability of the TPU electrodes over time was tested via cycling the electrode within $[Fe(CN)_6]^{4-}$ (1 mM in 0.1 M KCl) for 100 scans. Fig. 5E presents the 1st and 100th scan of this process, where there is no significant change in the oxidation peak current or potential, indicating the stability of the electrode and minimal impact the aqueous environment or electrochemical process has on the material. Finally, due to the issues outlined above, all PLA based sensors tend to be a single-use item.
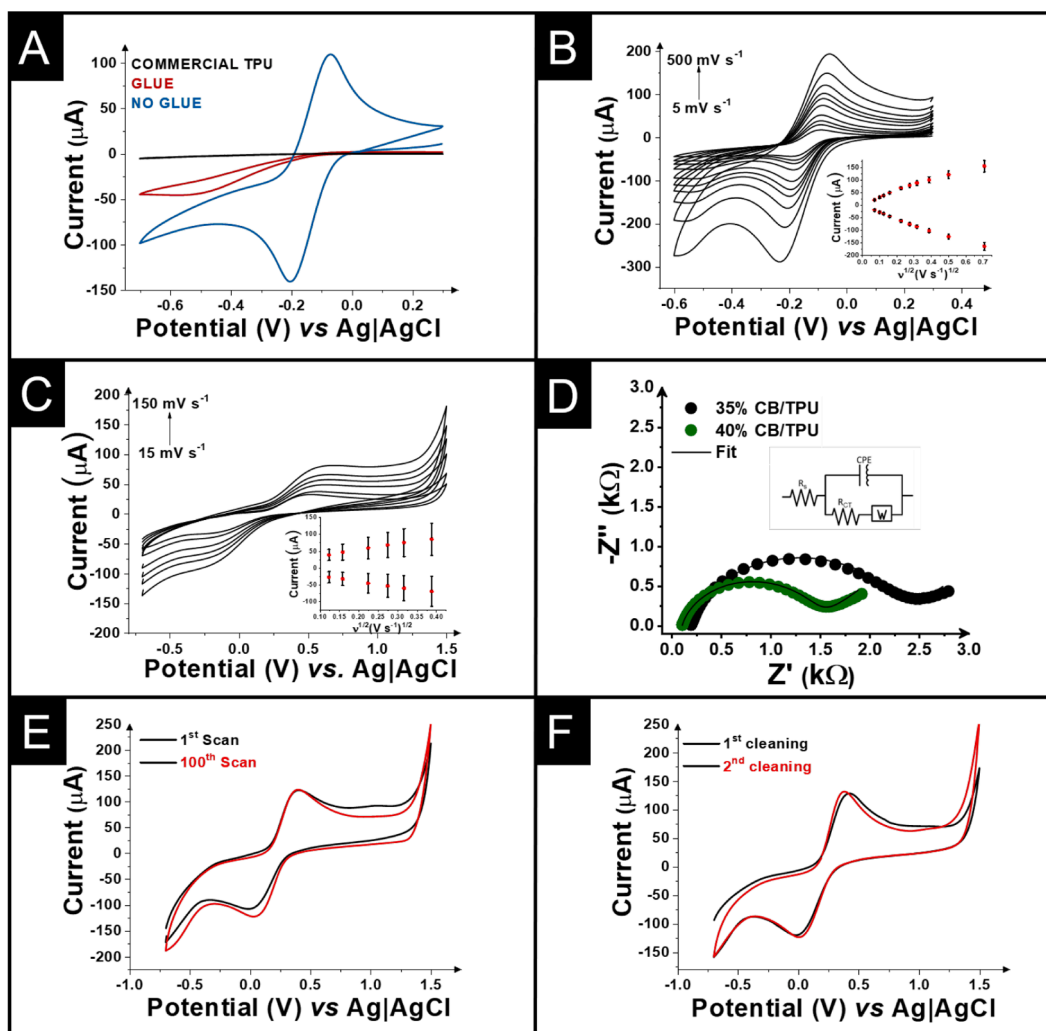
Fig. 5. A) Cyclic voltammograms (100 mV s^{-1}) of [Ru(NH$_3$)$_6$]$^{3+}$ (1 mM in 0.1 M KCl) with and without cleaning with 0.5 M NaOH solution using 35 wt% CB/TPU and comparison between the commercial filament. **B)** Scan rate study (5–500 mV s^{-1}) with [Ru(NH$_3$)$_6$]$^{3+}$ (1 mM in 0.1 M KCl) performed in the 40 wt% CB/TPU electrode. Inset: the Randles–Ševčík plot. **C)** Scan rate study (15–150 mV s^{-1}) with [Fe(CN)$_6$]$^{4-}$ (1 mM in 0.1 M KCl) performed in the 40 wt% CB/TPU electrode. Inset: the Randles–Ševčík plot. **D)** EIS Nyquist plots of [Fe(CN)$_6$]$^{4-/3-}$ comparing 35 wt% CB/TPU electrode with 40 wt% CB/TPU electrode. Inset: the proposed equivalent circuit. Comparison between **E)** the 1st and 100th cyclic voltammogram of [Fe(CN)$_6$]$^{4-}$ (1 mM in 0.1 M KCl). **F)** 1st and 2nd cleaning performed in the 40 wt% CB/TPU electrode. Scan rate: 100 mV s^{-1}.

Table 2

Summary of the electrochemical performance for the 35 wt% and 40 wt% CB/TPU electrodes.

	35 wt%	40 wt%
ΔE_p (mV)[1]	73 ± 4	84 ± 4
k^0 (x 10^{-3} cm s^{-1})[1]	1.61 ± 0.04	2.69 ± 0.10
ΔE_p (mV)[2]	629 ± 30	310 ± 29
k^0 (x 10^{-5} cm s^{-1})[2]	1.02 ± 0.17	58.5 ± 5.5
R_s (Ω)	162 ± 30	97 ± 7
R_{CT} (kΩ)	1910 ± 272	1550 ± 161

[1] : [Ru(NH$_3$)$_6$]$^{3+}$.
[2] : [Fe(CN)$_6$]$^{4-}$.

Therefore, to test the re-usability of the bespoke TPU electrodes, they were tested within [Fe(CN)$_6$]$^{4-}$ (1 mM in 0.1 M KCl) and then re-cleaned and tested once again. Fig. 5F shows the traces of the two cyclic voltammograms obtained where there is no significant difference in the responses, indicating that these electrodes can be reprocessed and used again.

3.5. Electrochemical performance of strained electrodes

We have seen in the previous section that our bespoke conductive TPU compares well with the best performing filaments from PLA, PETg and PP. However, the main focus for using TPU as the base polymer is to utilise the flexibility it can give to the finished prints. As such, electrochemical testing was investigated under strained conditions. Five additive manufactured holders were prepared at increasing angles (165, 150, 135, 120, and 105°) for the stem of the electrodes to be placed in (Figure S5). These electrodes were then tested using scan rate studies in both [Ru(NH$_3$)$_6$]$^{3+}$ and [Fe(CN)$_6$]$^{4-}$ to identify whether the strain imposed affected the electrochemical performance. Fig. 6 shows the cyclic voltammograms obtained for angles 1, 3 and 5, alongside a comparison between all of the angles at 50 mV s^{-1} in [Ru(NH$_3$)$_6$]$^{3+}$. The studies for angles 2 and 4 can be found in Figure S6, with all of the plots in [Fe(CN)$_6$]$^{4-}$ found in Figure S7.

When observing Fig. 6, in particular Fig. 6D, it can be seen that there is no deterioration in the electrochemical performance of the electrodes when placed under strain. A summary of the electrochemical performance of the electrodes at different angles can be found in Table 3. Against both outer and inner sphere probes there is no significant change
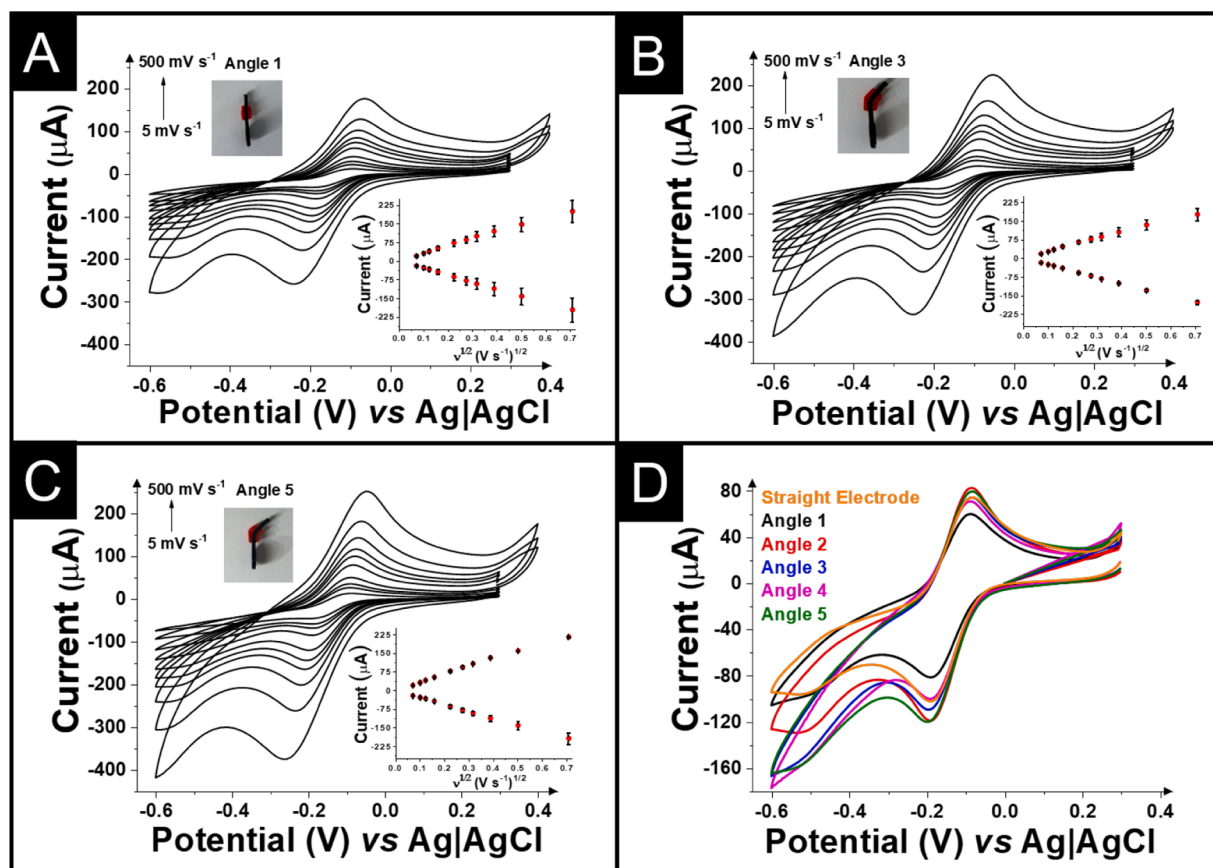
Fig. 6. Scan rate study (5–500 mV s^{-1}) with [Ru(NH$_3$)$_6$]$^{3+}$ (1 mM in 0.1 M KCl) performed in the 40 wt% CB/TPU electrode with different angles. Inset: the Randles–Ševčík plot: **A)** Angle 1; **B)** Angle 3; **C)** Angle 5; **D)** Comparison between cyclic voltammograms obtained from different angles and straight electrode (50 mV s^{-1}) of [Ru(NH$_3$)$_6$]$^{3+}$ (1 mM in 0.1 M KCl) using 40 wt% CB/TPU.

Table 3
Comparisons of the various electrochemical parameters, namely, heterogeneous electron transfer (k^0), electrochemically active area (A_e), EIS charge transfer resistance (R_{CT}) and solution resistance (R_S) for the different angles using bespoke 40 % CB/TPU electrodes.

	Angle 1	Angle 2	Angle 3	Angle 4	Angle 5
A_e (cm^2)[1]	0.34 ± 0.08	0.36 ± 0.03	0.31 ± 0.01	0.31 ± 0.05	0.40 ± 0.07
k^0 (x 10^{-3} cm s^{-1})[1]	2.69 ± 0.14	2.48 ± 0.26	2.48 ± 0.33	2.67 ± 0.11	2.12 ± 0.55
A_e (cm^2)[2]	0.59 ± 0.12	0.53 ± 0.03	0.65 ± 0.08	0.57 ± 0.08	0.57 ± 0.06
k^0 (x 10^{-4} cm s^{-1})[2]	1.67 ± 0.12	1.35 ± 0.13	1.59 ± 0.77	1.39 ± 0.49	1.65 ± 0.83
R_S (Ω)	95 ± 9	116 ± 8	121 ± 7	113 ± 9	114 ± 10
R_{CT} (kΩ)	1.72 ± 0.06	1.13 ± 0.07	1.89 ± 0.32	1.65 ± 0.16	1.60 ± 0.18

[1] : [Ru(NH$_3$)$_6$]$^{3+}$.
[2] : [Fe(CN)$_6$]$^{4-}$.

in either k^0 indicating that these electrodes perform reliably under different degree of strained conditions.

To complete the electrochemical characterisation of the strained electrodes, EIS was further carried out and the results obtained are depicted in Figure S8. In good agreement with the cyclic voltammetry, it is demonstrated that the electrodes performed well in the 5 different angles for both the R_S and R_{CT}. These results show the excellent promise this material has for use within additive manufactured flexible electronics and sensors.

3.6. Application to multianalyte detection of dopamine, uric acid, and nitrite in urine

Once electrochemically benchmarked and shown to be an excellent material for additive manufacturing electrochemistry, we turn to the materials' performance toward electroanalysis. To fully test the capabilities of the CB/TPU we look to perform the multianalyte detection of dopamine (DA), uric acid (UA) and nitrite (NIT) with the electrode bent at the highest angle tested above. These are all important biologically relevant molecules that can be found within human biological fluids, such as sweat and urine. To begin, analytical curves were produced for each of the analytes individually using differential pulse voltammetry in PBS (0.01 M, pH = 7.5), which can be found in Figure S9. It was observed that DA had two linear ranges, between 0.1–0.7 μM (Figure S9A) and 10–40 μM (Figure S9B), the first of which allowed for the determination of the limit of detection (LOD) utilising 3 times the standard deviation of the baseline divided by the sensitivity of the curve, which resulted in 11 nM. For UA there was a single linear range between 5–100 μM (Figure S9C), with an LOD of 0.53 μM, and for NIT a range between 10–50 μM (Figure S9D) and an LOD of 8.4 μM was calculated. Once individually analysed it was observed that the different values of peak potentials were separated enough to perform a further simultaneous detection of DA, UA and NIT. Then, a calibration curve for the multianalyte detection was successfully produced, as shown in Fig. 7.

Fig. 7A shows the voltammograms obtained for the simultaneous determination of DA, UA and NIT, where there is clear resolution between all three peaks. In particular, the resolution between dopamine and uric acid provides excellent evidence towards the electroanalytical performance of the CB/TPU. Fig. 7B-D show the calibration plots obtained from this simultaneous determination. DA was found to have a
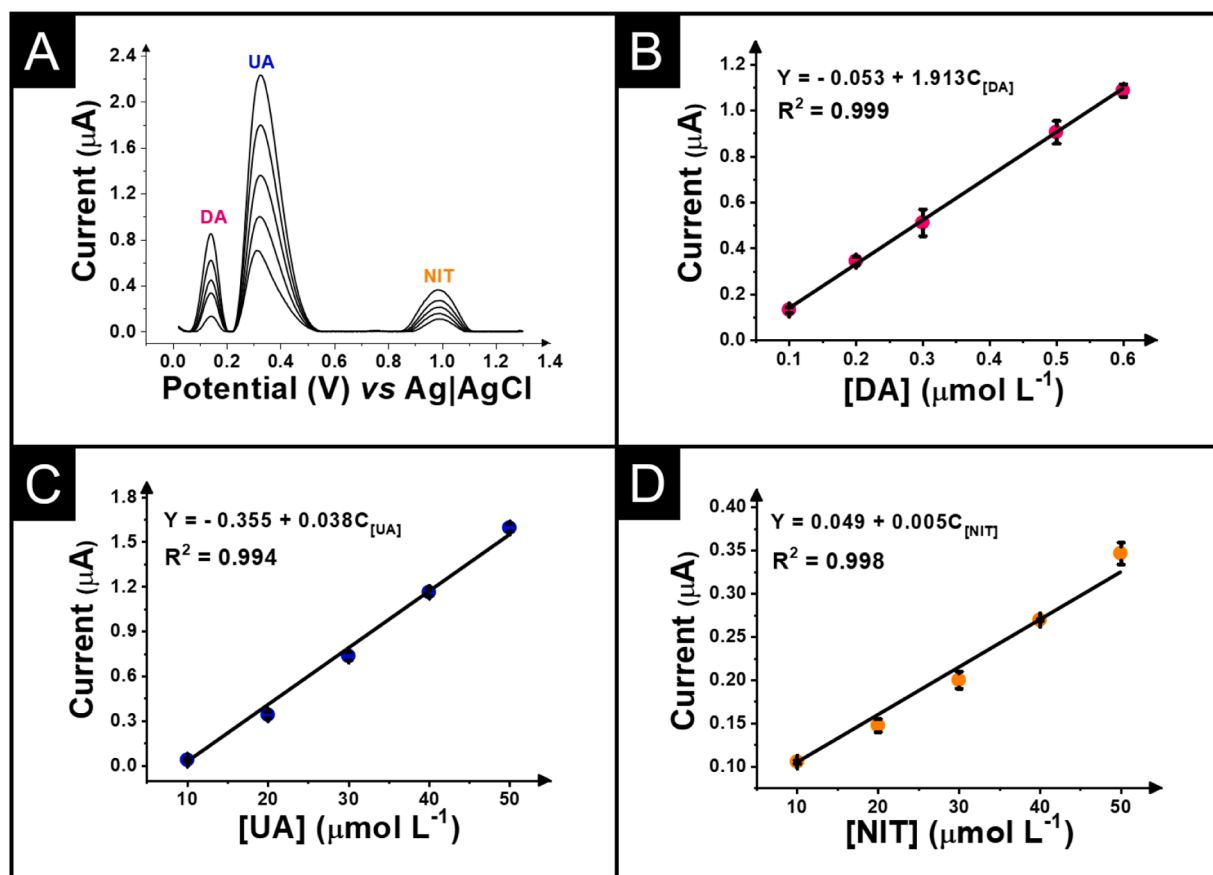
Fig. 7. A) Differential pulse voltammetry of dopamine (DA), uric acid (UA) and nitrite (NIT) simultaneously in different concentration in 0.01 M PBS recorded at 40 wt% CB/TPU (Angle 5) electrode. Respective calibration curves obtained simultaneously for: **B)** Dopamine; **C)** Uric Acid; and **D)** Nitrite. Step potential: 4 mV. Amplitude: 50 mV.

linear range between 0.1–0.6 µM, UA between 10–60 µM and NIT between 10–60 µM. R^2 values of 0.999, 0.994, and 0.998 were obtained for DA, UA, and NIT, respectively, again indicating the excellent electroanalytical performance of the CB/TPU electrode.

Last, to complete the electroanalytical application of the bespoke CB/TPU electrodes, further simultaneous determination of these analytes was performed in synthetic urine. The results obtained for the standard addition calibration of DA, UA and NIT in urine are shown in Fig. 8.

Within the synthetic urine, as in the buffer solution, there is clear separation of the differential pulse voltammetry peaks for dopamine, uric acid and nitrite, as depicted in Fig. 8A. The sequential additions of the three analytes standards produced great linear calibration curves (Fig. 8B-D) that were used along with these spiked urine samples to calculate recovery values, with DA and UA showing excellent recoveries of 107 % and 103 %, respectively. The recovery value for NIT was found to be higher at 139 %, indicating that some matrix effects may be seen. Nevertheless, these results show that the simultaneous detection of 3 important molecules, dopamine, uric acid and nitrite, with great biological interest is possible using our bespoke 40 wt% CB/TPU additive-manufactured electrodes, even while the sensor remains bent to the highest angle tested.

This paper shows the production of a highly conductive CB/TPU filament for use in additive manufacturing electrochemistry that offers excellent electrochemical and electroanalytical performance even when bent. This highly flexible and high performing filament has the potential to open up the field of bespoke wearable sensors for healthcare and monitoring applications.

4. Conclusions

In this work, we report the development of a flexible and highly conductive CB/TPU filament for use within additive manufacturing electrochemistry. The CB filler content was optimised at 40 wt%, achieving the best compromise between electrochemical performance, flexibility, and printability. The filaments and electrodes printed from this filament were physicochemically characterised through TGA, contact angle measurements, Raman spectroscopy, XPS, and SEM analysis, where the presence of the appropriate levels of CB conductive filler were confirmed. The electrodes were then electrochemically characterised, producing a k^0 of 2.69×10^{-3} cm s^{-1} outperforming most bespoke filaments in the literature across various base polymers. Importantly, the electrodes demonstrated stability over at least 100 scans and could be cleaned and re-used with no decrease in response. Furthermore, electrochemical testing whilst bending the electrodes at 5 different angles showed no deterioration of performance was observed toward either inner or outer sphere redox probes, highlighting the material's suitability for flexible electronics applications. Of note, we demonstrate that within the use of additive manufacturing technology, the choice of printer is key to avoid print failure; using a distance from extruder gears to nozzle, namely the filament path, as short as possible results in more reproducible additive manufacturing. Finally, the electrodes even at maximum bending angle, were used for the determination of dopamine, uric acid, and nitrite, with individual LODs of 11 nM, 0.53 µM, and 8.4 µM, respectively. Such strained electrodes were also successfully applied for the simultaneous determination of these analytes within buffer and synthetic urine, where good recovery values were obtained. This work presents a robust, highly conductive flexible filament for additive
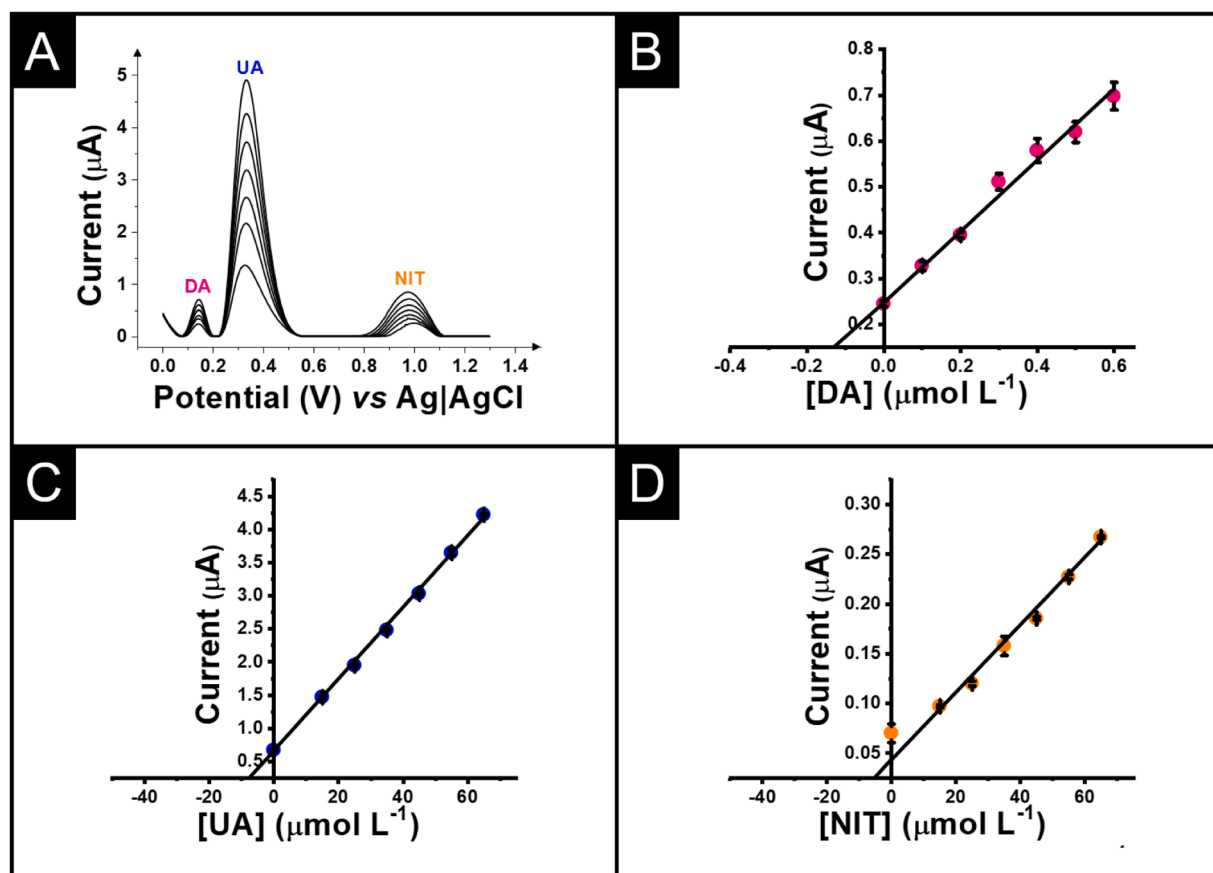
Fig. 8. A) Differential pulse voltammetry of dopamine, uric acid and nitrite recorded at 40 wt% CB/TPU (Angle 5) electrode and standard calibration plots for the determination of **B)** dopamine, **C)** uric acid and **D)** nitrite simultaneously in urine. Step potential: 4 mV. Amplitude: 50 mV.

manufacturing electrochemistry, demonstrating consistent performance even when bent. This advancement paves the way for integrating additive manufacturing electrochemistry into flexible electronics and wearable sensor technologies.

CRediT authorship contribution statement

Ana C.M. Oliveira: Formal analysis, Investigation, Methodology, Writing – original draft, Writing – review & editing. **Elena Bernalte:** Conceptualization, Formal analysis, Investigation, Methodology, Supervision, Writing – original draft, Writing – review & editing. **Robert D. Crapnell:** Conceptualization, Formal analysis, Investigation, Methodology, Supervision, Writing – original draft, Writing – review & editing. **Matthew J. Whittingham:** Software. **Rodrigo A.A. Muñoz:** Writing – original draft, Writing – review & editing, Funding acquisition, Supervision. **Craig E. Banks:** Conceptualization, Formal analysis, Funding acquisition, Project administration, Resources, Supervision, Writing – original draft, Writing – review & editing.

Declaration of competing interest

The authors declare that they have no known competing financial interests or personal relationships that could have appeared to influence the work reported in this paper.

Acknowledgements

Supplementary materials

Supplementary material associated with this article can be found, in the online version, at doi:10.1016/j.apmt.2025.102597.

Data availability

Data will be made available on request.

References

[1] M. Attaran, The rise of 3-D printing: the advantages of additive manufacturing over traditional manufacturing, Bus. Horiz. 60 (5) (2017) 677–688.
[2] K.R. Ryan, M.P. Down, C.E. Banks, Future of additive manufacturing: overview of 4D and 3D printed smart and advanced materials and their applications, Chem. Eng. J. 403 (2021) 126162.
[3] J. Muñoz, M. Pumera, Accounts in 3D-printed electrochemical sensors: towards monitoring of environmental pollutants, ChemElectroChem 7 (16) (2020) 3404–3413.
[4] R.M. Carvalho, V.S. Ferreira, B.G. Lucca, A novel all-3D-printed thread-based microfluidic device with an embedded electrochemical detector: first application in environmental analysis of nitrite, Anal. Meth. 13 (11) (2021) 1349–1357.
[5] A. Abdalla, B.A. Patel, 3D-printed electrochemical sensors: a new horizon for measurement of biomolecules, Curr. Opin. Electrochem. 20 (2020) 78–81.
[6] R.D. Crapnell, E. Bernalte, A.G.-M. Ferrari, M.J. Whittingham, R.J. Williams, N. J. Hurst, C.E. Banks, All-in-one single-print additively manufactured electroanalytical sensing platforms, ACS Measure. Sci. Au 2 (2) (2021) 167–176.
[7] N.C. de Moraes, E.N.T. da Silva, J.M. Petroni, V.S. Ferreira, B.G. Lucca, Design of novel, simple, and inexpensive 3D printing-based miniaturized electrochemical platform containing embedded disposable detector for analytical applications, Electrophoresis 41 (5–6) (2020) 278–286.

[8] S.V. Castro, R.G. Rocha, A.F. João, E.M. Richter, R. AA, Promising applications of additive-manufactured (3D-printed) electrochemical sensors for forensic chemistry, Braz. J. Anal. Chem. 9 (34) (2022) 79–105.

[9] A.F. João, R.G. Rocha, T.A. Matias, E.M. Richter, J.F.S. Petruci, R.A. Muñoz, 3D-printing in forensic electrochemistry: atropine determination in beverages using an additively manufactured graphene-polylactic acid electrode, Microchem. J. 167 (2021) 106324.

[10] R.G. Rocha, J.S. Ribeiro, M.H. Santana, E.M. Richter, R.A. Muñoz, 3D-printing for forensic chemistry: voltammetric determination of cocaine on additively manufactured graphene–polylactic acid electrodes, Anal. Meth. 13 (15) (2021) 1788–1794.

[11] R.D. Crapnell, A. Garcia-Miranda Ferrari, M.J. Whittingham, E. Sigley, N.J. Hurst, E.M. Keefe, C.E. Banks, Adjusting the connection length of additively manufactured electrodes changes the electrochemical and electroanalytical performance, Sensors 22 (23) (2022) 9521.

[12] A.G.-M. Ferrari, N.J. Hurst, E. Bernalte, R.D. Crapnell, M.J. Whittingham, D. A. Brownson, C.E. Banks, Exploration of defined 2-dimensional working electrode shapes through additive manufacturing, Analyst 147 (22) (2022) 5121–5129.

[13] A. Abdalla, B.A. Patel, 3D printed electrochemical sensors, Annu. Rev. Anal. Chem. 14 (1) (2021) 47–63.

[14] R.D. Crapnell, I.V.S. Arantes, J.R. Camargo, E. Bernalte, M.J. Whittingham, B. C. Janegitz, T.R.L.C. Paixão, C.E. Banks, Multi-walled carbon nanotubes/carbon black/rPLA for high-performance conductive additive manufacturing filament and the simultaneous detection of acetaminophen and phenylephrine, Microchim. Acta 191 (2) (2024) 96.

[15] C. Iffelsberger, C.W. Jellett, M. Pumera, 3D printing temperature tailors electrical and electrochemical properties through changing inner distribution of graphite/polymer, Small 17 (24) (2021) 2101233.

[16] R. Shergill, B. Patel, The effects of material extrusion printing speed on the conductivity of carbon black/polylactic acid electrodes, (2022).

[17] R.S. Shergill, C.L. Miller, B.A. Patel, Influence of instrument parameters on the electrochemical activity of 3D printed carbon thermoplastic electrodes, Sci. Rep. 13 (1) (2023) 339.

[18] R.S. Shergill, B.A. Patel, The effects of material extrusion printing speed on the electrochemical activity of carbon black/polylactic acid electrodes, ChemElectroChem 9 (18) (2022) e202200831.

[19] C. Kalinke, N.V. Neumsteir, G. de Oliveira Aparecido, T.V. de Barros Ferraz, P. L. Dos Santos, B.C. Janegitz, J.A. Bonacin, Comparison of activation processes for 3D printed PLA-graphene electrodes: electrochemical properties and application for sensing of dopamine, Analyst 145 (4) (2020) 1207–1218.

[20] D.P. Rocha, R.G. Rocha, S.V. Castro, M.A. Trindade, R.A. Munoz, E.M. Richter, L. Angnes, Posttreatment of 3D-printed surfaces for electrochemical applications: a critical review on proposed protocols, Electrochem. Sci. Adv. 2 (5) (2022) e2100136.

[21] R.S. Shergill, F. Perez, A. Abdalla, B.A. Patel, Comparing electrochemical pre-treated 3D printed native and mechanically polished electrode surfaces for analytical sensing, J. Electroanal. Chem. 905 (2022) 115994.

[22] R.D. Crapnell, C. Kalinke, L.R.G. Silva, J.S. Stefano, R.J. Williams, R.A.A. Munoz, J. A. Bonacin, B.C. Janegitz, C.E. Banks, Additive manufacturing electrochemistry: an overview of producing bespoke conductive additive manufacturing filaments, Mater. Today (2023).

[23] I.V. Arantes, R.D. Crapnell, M.J. Whittingham, E. Sigley, T.R. Paixão, C.E. Banks, Additive manufacturing of a portable electrochemical sensor with a recycled conductive filament for the detection of atropine in spiked drink samples, ACS Appl. Eng. Mater. 1 (9) (2023) 2397–2406.

[24] P. Wuamprakhon, R.D. Crapnell, E. Sigley, N.J. Hurst, R.J. Williams, M. Sawangphruk, E.M. Keefe, C.E. Banks, Recycled additive manufacturing feedstocks for fabricating high voltage, low-cost aqueous supercapacitors, Adv. Sustain. Syst. 7 (2) (2023) 2200407.

[25] R.D. Crapnell, I.V. Arantes, J.R. Camargo, E. Bernalte, M.J. Whittingham, B. C. Janegitz, T.R. Paixão, C.E. Banks, Multi-walled carbon nanotubes/carbon black/rPLA for high-performance conductive additive manufacturing filament and the simultaneous detection of acetaminophen and phenylephrine, Microchim. Acta 191 (2) (2024) 96.

[26] I.V. Arantes, R.D. Crapnell, E. Bernalte, M.J. Whittingham, T.R. Paixão, C.E. Banks, Mixed graphite/carbon black recycled PLA conductive additive manufacturing filament for the electrochemical detection of oxalate, Anal. Chem. 95 (40) (2023) 15086–15093.

[27] K.K. Augusto, R.D. Crapnell, E. Bernalte, S. Zighed, A. Ehamparanathan, J. L. Pimlott, H.G. Andrews, M.J. Whittingham, S.J. Rowley-Neale, O. Fatibello-Filho, Optimised graphite/carbon black loading of recycled PLA for the production of low-cost conductive filament and its application to the detection of β-estradiol in environmental samples, Microchim. Acta 191 (7) (2024) 375.

[28] C. Kalinke, R.D. Crapnell, E. Sigley, M.J. Whittingham, P.R. de Oliveira, L. C. Brazaca, B.C. Janegitz, J.A. Bonacin, C.E. Banks, Recycled additive

manufacturing feedstocks with carboxylated multi-walled carbon nanotubes toward the detection of yellow fever virus cDNA, Chem. Eng. J. 467 (2023) 143513.

[29] E. Koukouviti, A. Economou, C. Kokkinos, 3D printable multifunctional electrochemical nano-doped biofilament, Adv. Funct. Mater. (2024) 2402094.

[30] K.S. Erokhin, E.G. Gordeev, V.P. Ananikov, Revealing interactions of layered polymeric materials at solid-liquid interface for building solvent compatibility charts for 3D printing applications, Sci. Rep. 9 (1) (2019) 20177.

[31] R.J. Williams, T. Brine, R.D. Crapnell, A.G.-M. Ferrari, C.E. Banks, The effect of water ingress on additively manufactured electrodes, Mater. Adv. 3 (20) (2022) 7632–7639.

[32] E. Sigley, C. Kalinke, R.D. Crapnell, M.J. Whittingham, R.J. Williams, E.M. Keefe, B.C. Janegitz, J.A. Bonacin, C.E. Banks, Circular economy electrochemistry: creating additive manufacturing feedstocks for caffeine detection from post-industrial coffee pod waste, ACS Sustain. Chem. Eng. 11 (7) (2023) 2978–2988.

[33] R.D. Crapnell, I.V. Arantes, M.J. Whittingham, E. Sigley, C. Kalinke, B.C. Janegitz, J.A. Bonacin, T.R. Paixão, C.E. Banks, Utilising bio-based plasticiser castor oil and recycled PLA for the production of conductive additive manufacturing feedstock and detection of bisphenol A, Green Chem. (2023).

[34] J.R. Camargo, R.D. Crapnell, E. Bernalte, A.J. Cunliffe, J. Redfern, B.C. Janegitz, C. E. Banks, Conductive recycled PETg additive manufacturing filament for sterilisable electroanalytical healthcare sensors, Appl. Mater. Today 39 (2024) 102285.

[35] R.D. Crapnell, E. Bernalte, E. Sigley, C.E. Banks, Recycled PETg embedded with graphene, multi-walled carbon nanotubes and carbon black for high-performance conductive additive manufacturing feedstock, RSC Adv. 14 (12) (2024) 8108–8115.

[36] Z. Li, B. Li, B. Chen, J. Zhang, Y. Li, 3D printed graphene/polyurethane wearable pressure sensor for motion fitness monitoring, Nanotechnology 32 (39) (2021) 395503.

[37] Y. Mukai, S. Li, M. Suh, 3D-printed thermoplastic polyurethane for wearable breast hyperthermia, Fashion Text. 8 (2021) 1–12.

[38] A. Osman, J. Lu, 3D printing of polymer composites to fabricate wearable sensors: a comprehensive review, Mater. Sci. Eng.: R: Rep. 154 (2023) 100734.

[39] A. Frick, A. Rochman, Characterization of TPU-elastomers by thermal analysis (DSC), Polym. Test. 23 (4) (2004) 413–417.

[40] G. Greczynski, L. Hultman, The same chemical state of carbon gives rise to two peaks in X-ray photoelectron spectroscopy, Sci. Rep. 11 (1) (2021) 1–5.

[41] A.F. Stalder, G. Kulik, D. Sage, L. Barbieri, P. Hoffmann, A snake-based approach to accurate determination of both contact points and contact angles, Coll. Surf. A: Physicochem. Eng. Asp. 286 (1–3) (2006) 92–103.

[42] E.M. Richter, D.P. Rocha, R.M. Cardoso, E.M. Keefe, C.W. Foster, R.A. Munoz, C. E. Banks, Complete additively manufactured (3D-printed) electrochemical sensing platform, Anal. Chem. 91 (20) (2019) 12844–12851.

[43] P. Research, How to Trim PTFE Tube - Original Prusa Printers, 2024. https://help. prusa3d.com/guide/how-to-trim-ptfe-tube-original-prusa-printers_22424. Accessed 27/09/2024 2024.

[44] E3D, E3D Hemera - A Next Generation Extrusion System, 2019. Accessed 27/09/2024 2024.

[45] T.L. Barr, S. Seal, Nature of the use of adventitious carbon as a binding energy standard, J. Vac. Sci. Technol. A: Vac. Surf. Films 13 (3) (1995) 1239–1246.

[46] M.J. Glowacki, M. Cieslik, M. Sawczak, A. Koterwa, I. Kaczmarzyk, R. Jendrzejewski, L. Szynkiewicz, T. Ossowski, R. Bogdanowicz, P. Niedzialkowski, Helium-assisted, solvent-free electro-activation of 3D printed conductive carbon-polylactide electrodes by pulsed laser ablation, Appl. Surf. Sci. 556 (2021) 149788.

[47] R. Blume, D. Rosenthal, J.P. Tessonnier, H. Li, A. Knop-Gericke, R. Schlögl, Characterizing graphitic carbon with X-ray photoelectron spectroscopy: a step-by-step approach, ChemCatChem 7 (18) (2015) 2871–2881.

[48] T.R. Gengenbach, G.H. Major, M.R. Linford, C.D. Easton, Practical guides for x-ray photoelectron spectroscopy (XPS): interpreting the carbon 1s spectrum, J. Vac. Sci. Technol. A 39 (1) (2021).

[49] G. Socrates, Infrared and Raman characteristic Group frequencies: Tables and Charts, John Wiley & Sons, 2004.

[50] A. García-Miranda Ferrari, C.W. Foster, P.J. Kelly, D.A.C. Brownson, C.E. Banks, Determination of the electrochemical area of screen-printed electrochemical sensing platforms, Biosensors (Basel) 8 (2) (2018) 53.

[51] R.D. Crapnell, C.E. Banks, Perspective: what constitutes a quality paper in electroanalysis? Talanta Open 4 (2021) 100065.

[52] D.L.O. Ramos, R.D. Crapnell, R. Asra, E. Bernalte, A.C.M. Oliveira, R.A.A. Muñoz, E.M. Richter, A.M. Jones, C.E. Banks, Conductive polypropylene additive manufacturing feedstock: application to aqueous electroanalysis and unlocking nonaqueous electrochemistry and electrosynthesis, ACS Appl. Mater. Interf. 16 (41) (2024) 56006–56018.